Distinguishing dijet resonances at the LHC

R. Sekhar Chivukula, Elizabeth H. Simmons, and Natascia Vignaroli

Department of Physics and Astronomy, Michigan State University, East Lansing, Michigan 48824, USA
(Received 15 December 2014; published 18 March 2015)

Anticipating that a dijet resonance could be discovered at the 14 TeV LHC, we present two different strategies to reveal the nature of such a particle; in particular to discern whether it is a quark-antiquark ($q\bar{q}$), quark-gluon (qg), or gluon-gluon (gg) resonance. The first method relies on the color discriminant variable, which can be calculated at the LHC from the measurements of the dijet signal cross section, the resonance mass, and the resonance width. Including estimated statistical uncertainties and experimental resolution, we show that a qg excited quark resonance can be efficiently distinguished from either a $\bar{q}q$ coloron or a gg color-octet scalar using the color discriminant variable at LHC-14. The second strategy is based on the study of the energy profiles of the two leading jets in the dijet channel. Including statistical uncertainties in the signal and the QCD backgrounds, we show that one can distinguish, in a model-independent way, between gg, qg, and $q\bar{q}$ resonances; an evaluation of systematic uncertainties in the measurement of the jet energy profile will require a detailed detector study once sufficient 14 TeV dijet data are in hand.

I. INTRODUCTION

Searches for heavy resonances produced in the *s* channel and decaying into a pair of jets offer a simple and powerful probe of many different scenarios of new physics at the Large Hadron Collider. ATLAS [1] and CMS [2,3] have recently presented the results of the searches for narrow dijet resonances at the LHC with $\sqrt{s} = 8$ TeV. Lower limits on the masses of new hypothetical particles in a variety of beyond the standard model theories have been obtained. The upcoming LHC run at $\sqrt{s} = 14$ TeV will have the capability to greatly extend the discovery reach in the dijet channel [4]. If a hadronic resonance is discovered in the dijet channel, a major challenge will be the identification of the nature and of the properties of the newly discovered particle. In this work we present two different strategies to reveal if such a particle is a quark-antiquark ($\bar{q}q$), a quark-gluon (qg), or a gluon-gluon (gg) resonance. The first method uses the recently introduced color discriminant variable [5]. The second strategy analyzes the energy profiles of the two final jets [6].

The color discriminant variable reflects the color structure of the resonance and can be calculated at the LHC from the measurements of the dijet signal cross section, the resonance mass, and the resonance width. We present in this work the values of this variable for $\bar{q}q$, qg, and gg resonances in a wide resonance mass range, including the estimates of statistical and systematic uncertainties. We consider three compelling benchmark scenarios to describe the different dijet resonances: the flavor universal coloron model [7,8] for $\bar{q}q$ resonances, the excited quark model of Refs. [9,10] for qg resonances, and the general parametrization in [11] of color-octet scalar interactions for gg resonances. All of the results are shown in the relevant mass-coupling parameter space that both is not excluded by

the 8 TeV LHC analyses [1–3] and is conducive to a 5σ discovery of the resonance in the dijet channel at the 14 TeV LHC. The LHC-8 excluded regions are extracted from the ATLAS [1] and CMS [2,3] searches; the LHC-14 discovery reach is evaluated based on Monte Carlo (MC) simulations.

Additional and complementary information on the partonic origin of a dijet resonance is provided by the analysis of the jets' substructure, in particular by the study of the energy profiles [6] of the two final jets. Quark-initiated jets have more quickly rising profiles compared to gluon jets, so that discrimination among the different $\bar{q}q$, qg, and gg dijet resonances is possible from analyzing the dijet energy profiles. We evaluate the (mean) jet energy profiles by applying the theoretical calculations in perturbative QCD, at next-to-leading logarithmic accuracy, which have been developed in Refs. [12,13]. Statistical fluctuations on the jet energy profiles are generated through Monte Carlo simulations and, consequently, the statistical efficiency of our discriminating tool based on the dijet energy profiles is evaluated. Including statistical uncertainties in the signal and the background, we show that one can distinguish between gg, qg, and $q\bar{q}$ resonances in a model-independent way; an evaluation of systematic uncertainties in the measurement of the jet energy profile will require a detailed detector study once sufficient 14 TeV dijet data are in hand and is beyond the scope of this paper.

Additional techniques based on the study of jet substructure and aimed at identifying dijet resonances and/or improving the signal-to-background ratio have been extensively considered in the literature. Recent examples are the study of the color flow in Ref. [14], the analysis of the charge track multiplicity and the p_T-weighted linear radial moment (girth) in Refs. [15–17], and the study of generalized angularities in [18] aimed at distinguishing quark

and gluon jets on an event-by-event basis. The current status of jet substructure techniques, covering both experimental and theoretical efforts, is reviewed in [19].

The rest of the paper is organized as follows: we present the three benchmark models for $\bar{q}q$, gg, qg dijet resonances in Sec. II. In Sec. III we present the 14 TeV LHC discovery reach for the different types of dijet resonances. The prospects for distinguishing between $\bar{q}q$, qg, gg resonances through the color discriminant variable and through the study of jet energy profiles are shown in Sec. IV and in Sec. V, respectively. We draw our conclusions in Sec. VI.

II. BENCHMARK MODELS FOR DIJET RESONANCES

We consider three benchmark models for $\bar{q}q$, qg, and gg resonances. For gg and qg resonances, we will refer to the same models as were considered in the recent CMS [2,3] and ATLAS [1] analyses. For the $\bar{q}q$ resonance, we will consider the flavor universal coloron model considered in the CMS analysis [2,3].

A. Flavor universal colorons (*C*)

Quark-antiquark resonances are present in many different kinds of new physics scenarios. Color-singlet vector bosons Z' and W' can decay into quark pairs, as can new color-octet vector bosons, coming from extradimensional theories or from models with new strongly interacting dynamics. We will consider this latter case in this paper; specifically we focus on the coloron model presented in Refs. [7,8]. This model belongs to the class of theories predicting an extended strongly interacting sector $SU(3)_1 \times SU(3)_2$ that spontaneously breaks to $SU(3)_{\text{QCD}}$ [20–22]. The model can be flavor universal, which is the case we will consider here. Compelling alternatives that realize next-to-minimal flavor violation, where the coloron couples more strongly to third generation quarks, have also been studied in the literature [23]. We will leave to future studies the possibility of distinguishing the different coloron flavor structures at the LHC.[1]

We will now briefly review the flavor-universal coloron model [7,8]. At high energies, the model features an enlarged color gauge structure $SU(3)_1 \times SU(3)_2$. This extended color symmetry is broken down to $SU(3)_C$ by the (diagonal) expectation value of a scalar field, which transforms as a $(\mathbf{3}, \bar{\mathbf{3}})$ under $SU(3)_1 \times SU(3)_2$. It is assumed that each standard model (SM) quark transforms as a $(\mathbf{1}, \mathbf{3})$ under the extended strong gauge group. The color symmetry breaking induces a mixing between the original $SU(3)_1$ and $SU(3)_2$ gauge fields, which is diagonalized by a field rotation determined by

$$\tan\theta = \frac{g_2}{g_1}, \qquad g_S = g_1 \sin\theta = g_2 \cos\theta, \qquad (1)$$

where g_S is the QCD strong coupling and g_1, g_2 are the $SU(3)_1$ and $SU(3)_2$ gauge couplings, respectively. The diagonalization reveals two classes of color-octet vector boson mass eigenstates—the massless SM gluons and the new colorons C^a, which are massive,

$$m_C = \frac{g_S u}{\sin\theta \cos\theta}, \qquad (2)$$

where u is the breaking scale for the extended color symmetry. The coloron's interactions with quarks are determined by a new QCD-like coupling

$$-g_S \tan\theta \sum_f \bar{q}_f \gamma^\mu \frac{\lambda^a}{2} q_f C^a_\mu. \qquad (3)$$

A coloron that decays to all six quark flavors ($m_c > 2m_{top}$) has a decay width

$$\Gamma(C) = \alpha_S m_C \tan^2\theta. \qquad (4)$$

Colorons can be produced at the LHC by quark-antiquark fusion at a rate determined by the C coupling to light quarks, $g_s \tan\theta$. Gluon-gluon fusion production, on the other hand, is forbidden at tree level by $SU(3)_C$ gauge invariance [25–27], and has been found to be insignificant at the one-loop level [28]. The CMS search for dijet resonances [2,3] has considered the hypothesis of a flavor universal coloron, taking this model as a benchmark and fixing $\tan\theta = 1$.

B. Excited quarks (*q**)

Quark-gluon resonances are a general prediction of composite models with excited quarks [9,10]. They also appear in composite Higgs models with specific flavor structures [29]. In this work we will take as our exemplar the phenomenological model of [9], which describes an electroweak doublet of excited color-triplet vectorlike quarks $q^* = (u^*, d^*)$ coupled to first-generation ordinary quarks. In this model, right-handed excited quarks interact with gauge bosons and ordinary (left-handed) quarks through magnetic moment interactions described by the effective Lagrangian

$$\mathcal{L}_{\text{int}} = \frac{1}{2\Lambda} \bar{q}^*_R \sigma^{\mu\nu} \left[g_S f_S \frac{\lambda^a}{2} G^a_{\mu\nu} + g f \frac{\boldsymbol{\tau}}{2} \cdot \mathbf{W}_{\mu\nu} + g' f' \frac{Y}{2} B_{\mu\nu} \right] q_L$$
$$+ \text{H.c.} \qquad (5)$$

The excited quarks can decay into qg or into a quark plus a gauge boson. The corresponding decay rates are

---

[1]A first study in this direction is presented in Ref. [24], which has discussed a method to discriminate between flavor-nonuniversal colorons and Z' bosons.

$$\Gamma(q^* \to qg) = \frac{1}{3}\alpha_S f_S^2 \frac{m_{q*}^3}{\Lambda^2},$$

$$\Gamma(q^* \to q\gamma) = \frac{1}{4}\alpha f_\gamma^2 \frac{m_{q*}^3}{\Lambda^2},$$

$$\Gamma(q^* \to qV)) = \frac{1}{8}\frac{g_V^2}{4\pi}f_V^2 \frac{m_{q*}^3}{\Lambda^2}\left[1 - \frac{m_V^2}{m_{q*}^2}\right]^2 \left[2 + \frac{m_V^2}{m_{q*}^2}\right] \quad (6)$$

with $V = W, Z$ and with the definitions

$$f_\gamma = fT_3 + f'\frac{Y}{2},$$

$$f_Z = fT_3\cos^2\theta_W - f'\frac{Y}{2}\sin^2\theta_W,$$

$$f_W = \frac{f}{\sqrt{2}}. \quad (7)$$

The $q^* \to qg$ branching ratio is about 0.8 for $f_S = f = f'$.

Excited quarks are singly produced at the LHC through quark-gluon annihilation and, as just noted, they dominantly decay into qg. For our analysis, we choose the benchmark parameters $\Lambda = m_{q^*}$ and $f_S = f = f'$, while allowing the overall coupling strength to vary. By way of comparison, recent LHC searches, CMS [2,3], and ATLAS [1] have used the same value of Λ with $f_S = f = f' = 1$.

C. Color-octet scalars (S_8)

A gluon-gluon final state can generally arise from decay of colored scalars in models with extended color gauge structures [20–22,30,31]. In this work we adopt the general effective interaction for a color octet scalar, S_8, introduced in [11],

$$\mathcal{L}_{S_8} = g_S d^{ABC} \frac{k_S}{\Lambda_S} S_8^A G_{\mu\nu}^B G^{C,\mu\nu}, \quad (8)$$

where d is the QCD totally symmetric tensor.

A colored scalar of this kind is singly produced at the LHC through gluon-gluon annihilation. We consider the case in which it decays entirely (or almost entirely) into gluons. The corresponding decay rate reads

$$\Gamma(S_8) = \frac{5}{3}\alpha_S \frac{k_S^2}{\Lambda_S^2} m_{S_8}^3. \quad (9)$$

We set $\Lambda_S = m_{S_8}$, and we present results for different couplings k_S. Similarly, CMS [2,3] and ATLAS [1] present searches for $\Lambda_S = m_{S_8}$ and $k_S = 1$.

III. LHC DISCOVERY REACH

For each type of dijet resonance, we begin by deriving the relevant mass and coupling parameter space for our analysis, namely the region that is not yet excluded by

LHC-8 analyses and in which a 5σ discovery will be possible at the 14 TeV LHC.

We derive the excluded parameter region for colorons from the CMS analysis in [2]; for excited quarks and scalar octets, we obtain constraints by considering the strongest limits within the CMS [2] and ATLAS analyses [1]. Note that CMS and ATLAS searches in the dijet mass spectrum have a poor sensitivity to resonances whose width is large compared to the detector dijet mass resolution, i.e., with a width-over-mass value of greater than $\sim$0.15 [32].[2] In what follows, we assume that the new resonances are sufficiently narrow to be discovered in the dijets mass spectrum and that they decay only (or at least predominantly) to pairs of jets: $\bar{q}q$, qg, or gg.

The 5σ discovery reach at the 14 TeV LHC is estimated by evaluating $S/\sqrt{S+B}$, where S and B are, respectively, the total number of signal and background dijet events passing the CMS kinematic selection criteria in [2],

$$p_T(j_{1,2}) > 30\,\text{GeV}, \quad |\eta(j_{1,2})| < 2.5, \quad |\Delta\eta(j_1 j_2)| < 1.3. \quad (10)$$

For a given potential resonance mass M we also require the invariant mass of the two leading jets to be within a range of $\pm 0.15M$ from the dijet invariant mass peak. The standard model dijet background is taken from Ref. [38], where it has been carefully estimated by applying the same CMS cuts to matched samples of two- and three-jet final states using MADGRAPH [39] and PYTHIA [40]. The simulated dijet signals at the 14 TeV LHC for the different resonances are generated at parton level with MADGRAPHv5 and the CT10 [41] set of parton distribution functions, after implementing the benchmark models with FEYNRULES [42]. We find an acceptance rate for the CMS kinematic selection criteria [2] of about 0.58 for S_8 or q^* and of about 0.5 for C, for the mass ranges of interest.

Figure 1 shows our estimates of the 5σ reach at the 14 TeV LHC in the mass-vs-coupling plane for colorons, excited quarks, and scalar octets, for integrated luminosities of 30–3000 fb^{-1}. The discovery reach we find for the coloron is very similar to those already derived in [38,43] and in [5].

Within each pane of Fig. 1, we may identify a "region of interest" where a resonance of a given mass and coupling is not excluded by LHC (i.e., is not in the blue region at left), is relatively narrow (lies below the horizontal dashed curve), and would be detectable at LHC-14 at the indicated luminosity (is within the central light-grey region). We

---

[2]A broad resonance nevertheless could be detected in different channels or even in the dijet final state by considering supplementary strategies, like the analysis of the dijet angular distribution recently considered by CMS [33]. If the heavy resonance can decay into new states, like top partners in composite Higgs models, new search strategies focused on the new states also become important [34–37].
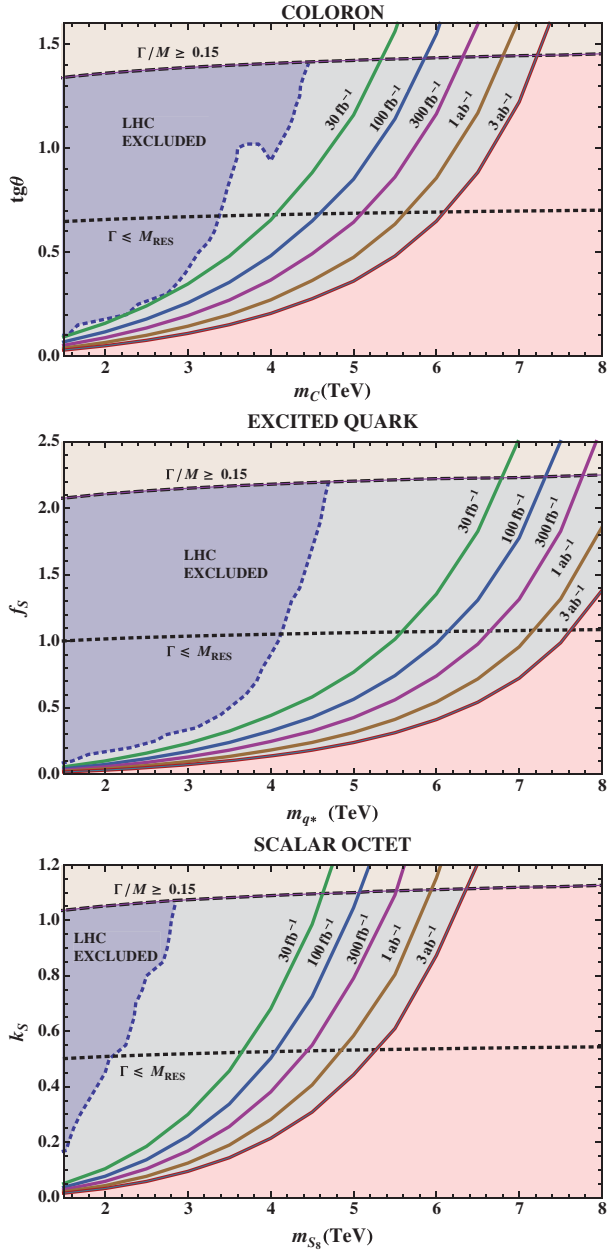
FIG. 1 (color). In each pane from left to right: regions of coupling-mass parameter space excluded by LHC-8 (blue), regions accessible to LHC-14 (pale grey), region inaccessible at LHC-14 (pink). Thick colored curves show the 5σ reach at luminosities from 30 to 3000 fb^{-1}. Above the upper dashed line, the resonance is too broad to detect ($\Gamma = 0.15M$); below the lower dotted line it is narrower than the experimental resolution ($\Gamma \leq M_{\text{res}}$), where $M_{\text{res}} = 0.035M$ [2]. Resonance widths are calculated as shown in Sec. II.

shall see that the portion of this region of interest that lies above the horizontal dotted curve is accessible to coloron discriminant variable analysis, while the area below the dotted curve region is also accessible to jet energy profile analysis.

IV. THE COLOR DISCRIMINANT VARIABLE

The color discriminant variable was introduced in [5] as a means for telling apart color-singlet and color-octet $\bar{q}q$ resonances. Here, we employ it as a tool for distinguishing among dijet resonances decaying $\bar{q}q$, qg, or gg. The color discriminant variable is defined as

$$D_{\text{col}} = \frac{\sigma_{jj} M^3}{\Gamma}, \tag{11}$$

where σ_{jj} is the cross section times the dijet branching ratio for a heavy resonance of mass M and total decay width Γ. Note that D_{col} is dimensionless in the units $\hbar = c = 1$.

We evaluate the value of D_{col}—more precisely we calculate the $\log_{10} D_{\text{col}}$—for the three types of dijet resonances–flavor universal colorons, excited quarks, and scalar octets–in the allowed and accessible range of resonance masses. The dependence of D_{col} on the dijet mass is controlled by the parton distribution functions (PDFs), since the quark and gluon parton content vary with the energy scale of the dijet process. We calculate the dijet resonance production cross section by using the CT10 [41] next-to-leading-order (NLO) PDF set with factorization and renormalization scales fixed at the resonance mass value.[3]

The measurement of D_{col} at the LHC is affected by the statistical and systematic uncertainties on measurements of the dijet cross section, the resonance mass, and the resonance width. Furthermore, D_{col} is experimentally accessible only if the mass resolution of the detector is less than the intrinsic width of the resonance. We include these uncertainties following the analysis of Ref. [5]. In particular, the uncertainty on D_{col} is given by

$$\left(\frac{\Delta D}{D}\right)^2 = \left(\frac{\Delta \sigma_{jj}}{\sigma_{jj}}\right)^2 + \left(3\frac{\Delta M}{M}\right)^2 + \left(\frac{\Delta \Gamma}{\Gamma}\right)^2,$$

$$\left(\frac{\Delta \sigma_{jj}}{\sigma_{jj}}\right)^2 = \frac{1}{N} + \epsilon_{\sigma\text{SYS}}^2,$$

$$\left(\frac{\Delta M}{M}\right)^2 = \frac{1}{N}\left[\left(\frac{\sigma_\Gamma}{M}\right)^2 + \left(\frac{M_{\text{res}}}{M}\right)^2\right] + \left(\frac{\Delta M_{\text{JES}}}{M}\right)^2,$$

$$\left(\frac{\Delta \Gamma}{\Gamma}\right)^2 = \frac{1}{2(N-1)}\left[1 + \left(\frac{M_{\text{res}}}{\sigma_\Gamma}\right)^2\right]^2 + \left(\frac{M_{\text{res}}}{\sigma_\Gamma}\right)^4\left(\frac{\Delta M_{\text{res}}}{M_{\text{res}}}\right)^2, \tag{12}$$

where N is the number of signal events, $\epsilon_{\sigma\text{SYS}}$ is the systematic uncertainty on the dijet cross section, σ_Γ is the

---

[3]We have checked that the variation of the color discriminant variable induced by the uncertainties on the CT10 PDF set is negligible. We have also found no significant difference in our results when using the MSTW2008nlo [44] PDF set. On the other hand, we have found significant variations, of order $\mathcal{O}(1)$, in the production cross section values for the scalar octet at heavier masses, $M \gtrsim 4$ TeV, when using the older leading-order CTEQ6L1 [45] PDF set.

standard deviation corresponding to the intrinsic width of the resonance ($\sigma_\Gamma \simeq \Gamma/2.35$ assuming a Gaussian distribution), M_{res} is the experimental dijet mass resolution, $(\Delta M_{\text{res}}/M_{\text{res}})$ is the uncertainty in the resolution of the dijet mass, and $(\Delta M_{\text{JES}}/M)$ is the uncertainty in the mass measurement due to uncertainty in the jet energy scale.

Following [5], we estimate systematic uncertainties from actual LHC results, where available, and assume that any future LHC run will be able to reach at least this level of precision. In particular, we use

$$\epsilon_{\sigma\text{SYS}} = 0.41 \,(14 \text{ TeV LHC } [46]),$$

$$M_{\text{res}}/M = 0.035 \,(8 \text{ TeV CMS } [2]),$$

$$\Delta M_{\text{res}}/M_{\text{res}} = 0.1 \,(8 \text{ TeV CMS } [3]),$$

$$(\Delta M_{\text{JES}}/M) = 0.013 \,(8 \text{ TeV CMS } [3]). \tag{13}$$

Figure 2 shows the $\log_{10} D_{\text{col}}$ values, including the statistical and systematic uncertainties, for the three types of dijet resonances q^*, C, S_8, as a function of the dijet resonance mass at the 14 TeV LHC for different integrated luminosities. We observe that an excited quark resonance can be efficiently distinguished from either a coloron or a scalar octet resonance by the color discriminant variable at the 14 TeV LHC. Discriminating between colorons and scalar octets using the color discriminant variable is more challenging, but we find it should be possible to establish a separation which ranges from $\sim2\sigma$ at $M \simeq 4$ TeV to $\sim3\sigma$ at $M \simeq 6$ TeV.

Additional strategies to separate these two kinds of dijet resonances will be important. In the next section we will examine the discriminating power of an analysis of the dijet energy profiles.
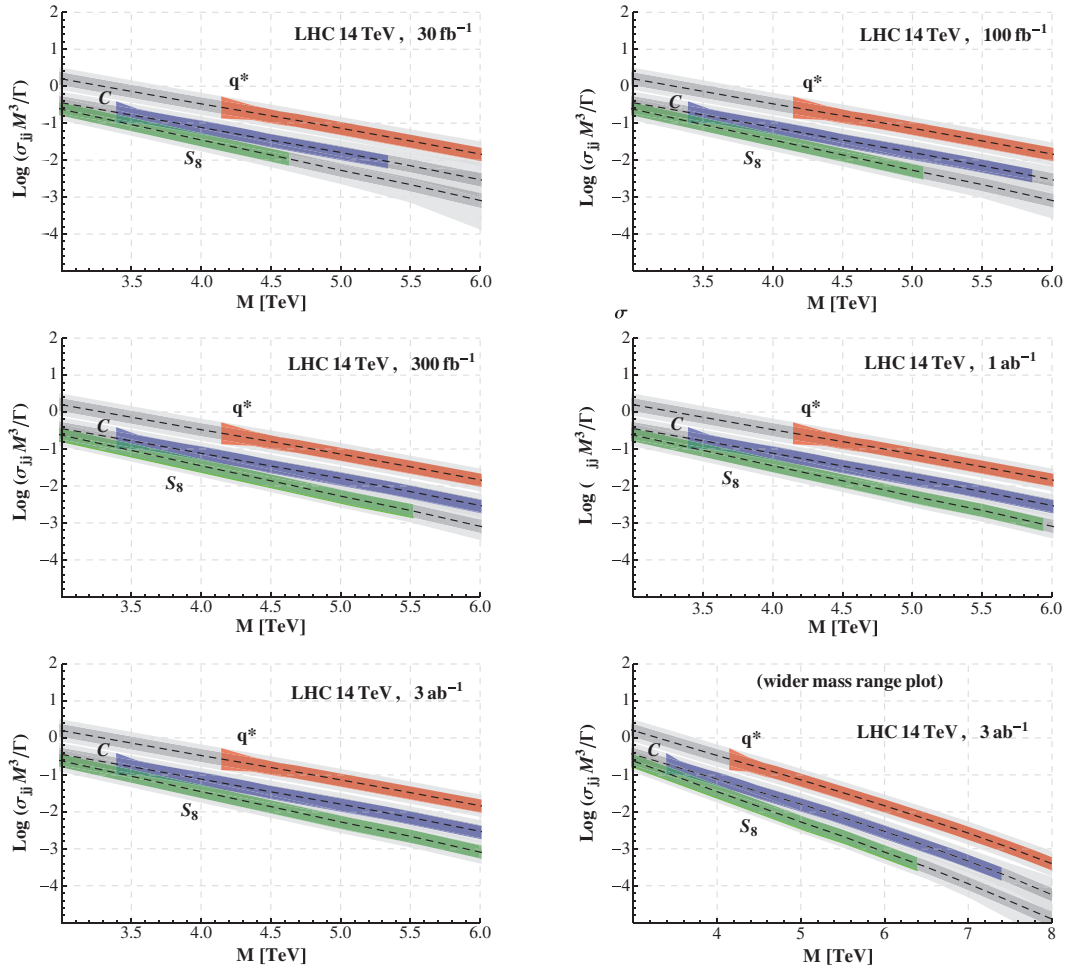

FIG. 2 (color).   Each pane shows $\log_{10} D_{\text{col}}$ for flavor universal colorons (C), excited quarks (q^*), and scalar octets (S_8) as a function of the dijet resonance mass at the 14 TeV LHC with a particular integrated luminosity. The outer (inner) grey (light grey) bands represent the ±1-sigma statistical plus systematic uncertainty on $\log_{10} D_{\text{col}}$ when the resonance width is narrow (broad): $\Gamma = M_{\text{res}}$ ($\Gamma = 0.15M$). The colored bands [red for $q*$, blue for (C), green for (S_8)] show the $\log_{10} D_{\text{col}} \pm 1\sigma$ values obtained in the region of parameter space where the resonance is allowed by LHC-8 analyses, is neither too broad nor too narrow, and is amenable to discovery at LHC-14, as discussed in Fig. 1 and at the end of Sec. III. The last pane redisplays the highest-luminosity plot to its left for a wider mass range.

V. JET ENERGY PROFILES

In this section we will examine the use of jet energy profiles (JEPs) [6] to statistically distinguish $\bar{q}q$, qg, and gg dijet resonances. This technique has also recently been applied to identify Higgs production mechanisms [47] and dark matter interactions [48]. For a jet of size R, the (integrated) JEP, $\psi(r)$, is defined as the fraction of jet transverse momentum that lies inside a subcone of size $r (< R)$,

$$\psi(r) = \frac{\sum_{r' < r} p_T(r')}{\sum_{r' < R} p_T(r')}. \tag{14}$$

Gluon-initiated jets radiate more and produce a slowly rising JEP. Quark initiated jets, on the other hand, radiate less and have a quickly rising JEP.

We will begin by considering the statistical limitations of measuring the JEP of a simulated sample of *pure* signal events—dijet events arising solely from a coloron, excited quark, or color-octet scalar. We will subsequently consider the effect of QCD background on the statistical significance of measuring the jet energy profile of the signal. We will show that the measurement is not statistically limited and, if systematic errors can be controlled, will clearly distinguish between the types of dijet resonances we consider. An evaluation of systematic uncertainties in the measurement of the jet energy profile will require a detailed detector study once sufficient 14 TeV dijet data are in hand, and this is beyond the scope of this paper.

A. JEP measurement based on signal events

We consider first the measurement of the jet energy profile of a sample of dijet events arising solely from the production of a coloron, excited quark, or color-octet scalar. As explained above, due to the differing pattern of soft gluon radiation from quarks and from gluons, in principle a measurement of the JEP could distinguish among these different types of resonances since they decay into different final states. Experimentally measured JEPs, of course, include not just the effects of the initial high-Q^2 radiation arising from the quarks and gluons produced in the hard event but also the subsequent low-Q^2 showering and hadronization of these objects—a description of which depends on tune-dependent Monte Carlo event generators such as PYTHIA [40,49]. JEPs have been recently measured at ATLAS [50] and at CMS [51] and, indeed, the results of the JEP measurements [50,51] show that the data can be reproduced only after a careful calibration of the shower/hadronization parameters.

The copious dijet data available from the 14 TeV LHC will allow for the necessary calibration—and, as we will show, we expect to find clear differences between the dijet JEP measured in the resonance region and that measured from the purely SM background events at off-resonance

dijet invariant masses. However, since 14 TeV LHC data and tuned event generators are not yet available, we will rely on a theoretical calculation to estimate the *average* shape of the JEPs for colorons, excited quarks, and color-octet scalars, and we will use MC simulations—MADGRAPH interfaced with PYTHIA v6.4 (default tune)—to evaluate the statistical uncertainties on the measurement of these profiles. Specifically, we calculate the mean values of the jet energy profiles in perturbative QCD (pQCD) by using the jet functions derived in [12,13], which apply a next-to-leading-logarithm (NLL) resummation.[4] Indeed, we find this procedure yields very good agreement with the experimental data from CMS at 7 TeV [51] and the Tevatron [52]. The pQCD calculation depends on two phenomenological parameters that take into account the effect of uncalculated sub-sub-leading logarithmic contributions. We will fix these parameters at the values that reproduce the Tevatron data [52]. Once calibration becomes possible, these parameters, too, will need to be fixed at the values that reproduce the 14 TeV LHC data.[5] Since we are not using calculations tuned to LHC energies, our *absolute* results for the jet energy profiles will not precisely match those to be expected at the LHC—however, we expect the *relative differences* in the JEPs we find between the various kinds of resonances to be representative of what would be seen there.

We consider first the signal of a 4 TeV dijet resonance, coming from an S_8, C, or q^*, which can be discovered with approximately 30 fb^{-1} at the 14 TeV LHC and which has not been excluded by the present LHC-8 searches. In particular, we consider an S_8 resonance with a coupling $k_S = 0.65$, a coloron with $\tan\theta = 0.6$ and a q^* with $f_S = 0.4$. After the CMS selection cuts (10), all of these three types of resonances give, approximately, the same signal cross section around the resonance peak. We will analyze the jet-energy profiles for dijet resonance events passing the CMS kinematic cuts (10) and appearing in a region $|M_{jj} - M| < \Gamma/2$; we take conservatively $\Gamma = \Gamma(S_8)$, corresponding to the largest possible width among those of the three types of resonances. The choice of focusing our analysis in a narrow region around the resonance peak is intended to minimize the SM dijet background which, as we will see in the next subsection, will affect the uncertainty of our discriminating tool. After selection we obtain a dijet resonance signal cross section of 22 fb.

The predicted JEPs for a quark or gluon jet, $\psi(r)$, are obtained as in Ref. [47] by fitting a functional form to the

---

[4]Terms of the form $\alpha_S^n (\log(R/r))^{2n}$, $\alpha_S^n (\log(R/r))^{2n-2}$ are resummed to all orders in α_S. The studies in [12,13] show that NLL resummation is necessary for a correct description of the data; fixed NLO calculations overestimate the JEPs and fail to describe the data.

[5]For example, Z +jets events with jets in a kinematic region similar to that of dijet resonances could be used as calibration samples.

results of a full perturbative QCD calculation done at several values of r.[6] Since the resonances we are studying each decay to two jets, we then calculate a predicted dijet profile ψ_{jj} for the resonance decay as

$$\psi_{jj}(r) = \psi_1(r) + \psi_2(r), \qquad (15)$$

where $\psi_1(r)$, $\psi_2(r)$, respectively, denote the JEPs of the leading and next-to-leading jet.

In order to quantify the power of JEPs to discriminate between different types of resonances, we will apply a one-parameter fit, so that we can unequivocally assign a specific value of the fit parameter to each signal dijet profile. Specifically, we can parametrize the generic dijet profile of the signal as

$$\psi_S(r) = f\psi_{\bar{q}q}(r) + (1 - f)\psi_{gg}(r). \qquad (16)$$

Here, f is our fit parameter that indicates the fraction of quark jets in a generic dijet resonance: $f = 0, 0.5, 1$ for a gg, qg, or $\bar{q}q$ resonance, respectively. The mean values of the different jet-energy profiles determined by pQCD are shown as the central values of the curves in Fig. 4—note the difference between the JEPs arising from $\bar{q}q$, qg, and gg dijet events.

We estimate the statistical uncertainty on the mean values of the JEPs for a sample of pure signal events by running pseudoexperiments through MC simulations. We evaluate the statistical errors in the JEPs at $\Delta r = 0.1$ steps. Signal sample events are generated with MADGRAPHv5 [39] and interfaced with PYTHIAv6 for shower and hadronization. The jets are clustered through FASTJET [53] by an anti-kT algorithm with cone size $R = 0.5$. JEPs are then obtained by analyzing the jet substructure, according to the formula in (14). We find, as expected, that the statistical fluctuations in ψ, and hence f, follow Gaussian distributions and that the errors scale as the square root of the number of events. In particular, we find that the uncertainty in the value of $\psi(r)$ at $r = 0.1$ (which yields the largest error) scales as

$$(\delta\psi_S(0.1))^2 \approx \frac{\sigma^2(0.1)}{S}, \qquad (17)$$

where $\sigma(0.1) \approx 0.4$ and S is the total number of signal events.
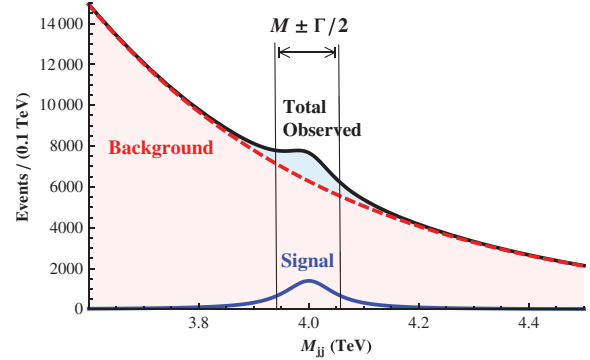

FIG. 3 (color).   Sketch of how the number of signal (blue curve), background (red dotted curve), and total observed events (black curve) could depend on dijet invariant mass (M_{jj}) if a dijet resonance is discovered at the LHC. This figure illustrates issues raised in the discussion of JEP measurements and uncertainties in Sec. VI B.

B. Including QCD background

Next, we consider the impact of QCD background on our analysis. The resonance will appear as a "bump" in a plot of the dijet invariant mass distribution, as sketched in Fig. 3. In the signal region ($|M_{jj} - M| < \Gamma/2$) there will be S signal events and B QCD background events. As mentioned above, for the benchmark 4 TeV dijet resonance we find a signal cross section of 22 fb, and extracting the background from Ref. [38], we find a signal-to-background ratio of 1/23.

It is not possible to measure the jet energy profile of the signal alone; measurements of the JEP in the signal region, $\psi_{OBS}(r)$, will include both signal and background. One can also measure the jet energy profiles in "sidebands," regions of dijet invariant mass immediately adjacent to but outside the resonance region; this yields an experimentally determined measurement of the JEP of the QCD background, $\psi_B(r)$. We expect that the experimental uncertainties on these individual measurements will scale analogously to what is shown in Eq. (17)[7]:

$$(\delta\psi_{OBS}(r))^2 \approx \frac{\sigma^2(r)}{S + B}, \qquad (\delta\psi_B(r))^2 \approx \frac{\sigma^2(r)}{B}. \quad (18)$$

The desired quantity $\psi_S(r)$ is now related to the measurable JEPs by

---

[6]To be more specific, the predicted $\psi(r)$ JEPs for either quark jets or gluon jets are obtained by fitting an exponential function of the type $(1 - be^{-ar})/(1 - be^{-aR})$ [47] to the discrete $\psi(r)$ values obtained from the full pQCD calculation at several fixed r points. We calculate $\psi(r)$ at $\Delta r = 0.1$ steps, starting from $r = 0.1$ up to $r = R = 0.5$.

[7]Note that we are implicitly assuming a sideband with a number of events comparable to the expected number of background events in the signal region. The choice of sideband could in principle be optimized: larger sidebands would reduce the statistical uncertainty while smaller sidebands would reduce the systematic error related to the background composition, which changes as a function of the dijet invariant mass. Finding the optimal compromise is beyond the scope of this paper, and we leave it to future dedicated studies.

$$\psi_{OBS}(r) = \frac{S}{S+B}\psi_S(r) + \frac{B}{S+B}\psi_B(r), \qquad (19)$$

and hence

$$\psi_S(r) = \psi_{OBS}(r) + \frac{B}{S}(\psi_{OBS}(r) - \psi_B(r)). \qquad (20)$$

The statistical uncertainties in the quantities ψ_{OBS} and ψ_B are given by Eq. (18). Since we are working in a regime in which $B \gg S$, the uncertainty in B/S is dominated by fluctuations in the number of signal events and is roughly $B/S^{3/2}$. From Eq. (20), we find the mean-square error on ψ_S to be

$$(\delta\psi_S)^2 \approx \frac{\sigma^2}{S}\left[1 + 2\frac{B}{S}\right] + \frac{(\psi_S - \psi_B)^2}{S}, \qquad (21)$$

where we have neglected terms suppressed by S/B. The first term in Eq. (21) represents the "dilution" in the measurement of ψ_S due to QCD background, relative to the sample-only error of Eq. (17), and the second term is due to the uncertainty in the number of signal events. From Fig. 4, we see that the difference in JEPs (which is maximal for the difference between pure qq and gg states at $r = 0.1$) is bounded from above by about 0.5; in the regions in which the dijet resonance can be observed, the second term in Eq. (21) is negligible. Figure 4 shows the resulting dijet energy profiles, with uncertainty bands including the effect of the background subtraction, for the $\bar{q}q$ (coloron), qg (excited quark), and gg (scalar octet) 4 TeV dijet resonance.

TABLE I. Estimated statistical precision for determining f values with 100 fb^{-1} at the LHC-14 for a 4 TeV flavor universal coloron with $\tan\theta = 0.6$ ($\bar{q}q$), an excited quark with $f_S = 0.4$ (qg), or a scalar octet with $k_S = 0.65$ (gg).

	f
$\bar{q}q$	1.00 ± 0.06
qg	0.50 ± 0.07
gg	0.00 ± 0.08

TABLE II. Expected distinction, in terms of σ level as shown in Eq. (22), between $\bar{q}q$-qg, gg-qg, and $\bar{q}q$-gg dijet resonances at 100 fb^{-1} of luminosity at the 14 TeV LHC (second column) and the amount of integrated luminosity, in inverse fb, required for a 5σ level distinction (third column). We consider a 4 TeV resonance corresponding to a scalar octet with $k_S = 0.65$, a flavor universal coloron with $\tan\theta = 0.6$ or an excited quark with $f_S = 0.4$. Note that the 30 fb^{-1} of integrated luminosity required for the discovery of the resonance is sufficient for a 5σ distinction between $\bar{q}q$ and gg.

	σ ($L = 100$ fb^{-1})	L (5σ)
$\bar{q}q$-qg	5.4	85
qg-gg	4.7	110
$\bar{q}q$-gg	10	30

We can translate the statistical error on $\psi(r)_S$ into a statistical uncertainty on the f parameter.[8] Results predicted for the 14 TeV LHC with 100 fb^{-1} of data are shown in Table I for 4 TeV dijet resonances.

We can finally evaluate the statistical efficiency of our discriminating tool according to a t test as

$$\sigma(\bar{q}q - gg) = \frac{\bar{f}_{\bar{q}q} - \bar{f}_{gg}}{\sqrt{\sigma^2(f_{\bar{q}q}) + \sigma^2(f_{gg})}},$$

$$\sigma(\bar{q}q - qg) = \frac{\bar{f}_{\bar{q}q} - \bar{f}_{qg}}{\sqrt{\sigma^2(f_{\bar{q}q}) + \sigma^2(f_{qg})}},$$

$$\sigma(qg - gg) = \frac{\bar{f}_{qg} - \bar{f}_{gg}}{\sqrt{\sigma^2(f_{qg}) + \sigma^2(f_{gg})}}, \qquad (22)$$
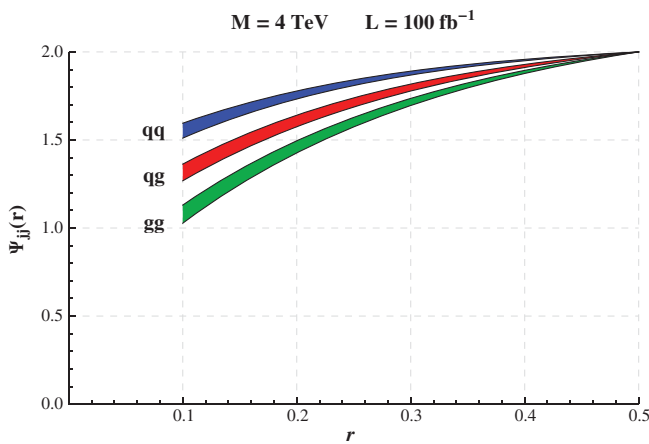

FIG. 4 (color). Dijet energy profiles for $\bar{q}q$ (coloron), qg (excited quark), and gg (scalar octet) 4 TeV dijet resonances (the respective resonance couplings are fixed to $\tan\theta = 0.6$, $f_S = 0.4$, and $k_S = 0.65$). Each band shows a $\pm 1\sigma$ statistical variation from the mean curve. The effect of background subtraction, Eq. (21), is included.

---

[8]This is obtained via the following procedure. Using a step size $\Delta r = 0.1$, we generate a large number of $\psi(r)$ values according to the Gaussian fluctuations which we have calculated by running pseudoexperiments. The generated $\psi(r)$ points are fitted by the function $(1 - be^{-ar})/(1 - be^{-aR})$ and the resulting profiles are translated into f values according to Eq. (16). We thus obtain the statistical fluctuation on f, and we are able to calculate the corresponding standard deviation.

where we take $\sigma(\bar{q}q - gg)$, $\sigma(\bar{q}q - qg)$, and $\sigma(qg - gg)$ as indicating the confidence level at which JEPs offer a distinction between $\bar{q}q$-gg, $\bar{q}q$-qg, and qg-gg resonances. Table II shows the expected number of confidence intervals at which the method will separate the different types of 4 TeV dijet resonances at the 14 TeV LHC. We find that even the most challenging discrimination, that between qg and gg resonances, can be performed at a high statistical level, of

$\sim 5\sigma$, with 100 fb^{-1} at the 14 TeV LHC. A $\bar{q}q$ resonance can be well distinguished from a gg resonance: a $\sim 5\sigma$ level of distinction can be achieved with only ~ 30 fb^{-1}.

We can repeat the above analysis for several different dijet resonance mass values and consequently estimate the statistical uncertainty on the quark-jet fraction parameter, Δf, for different resonance couplings and LHC luminosities by considering that Δf scales as
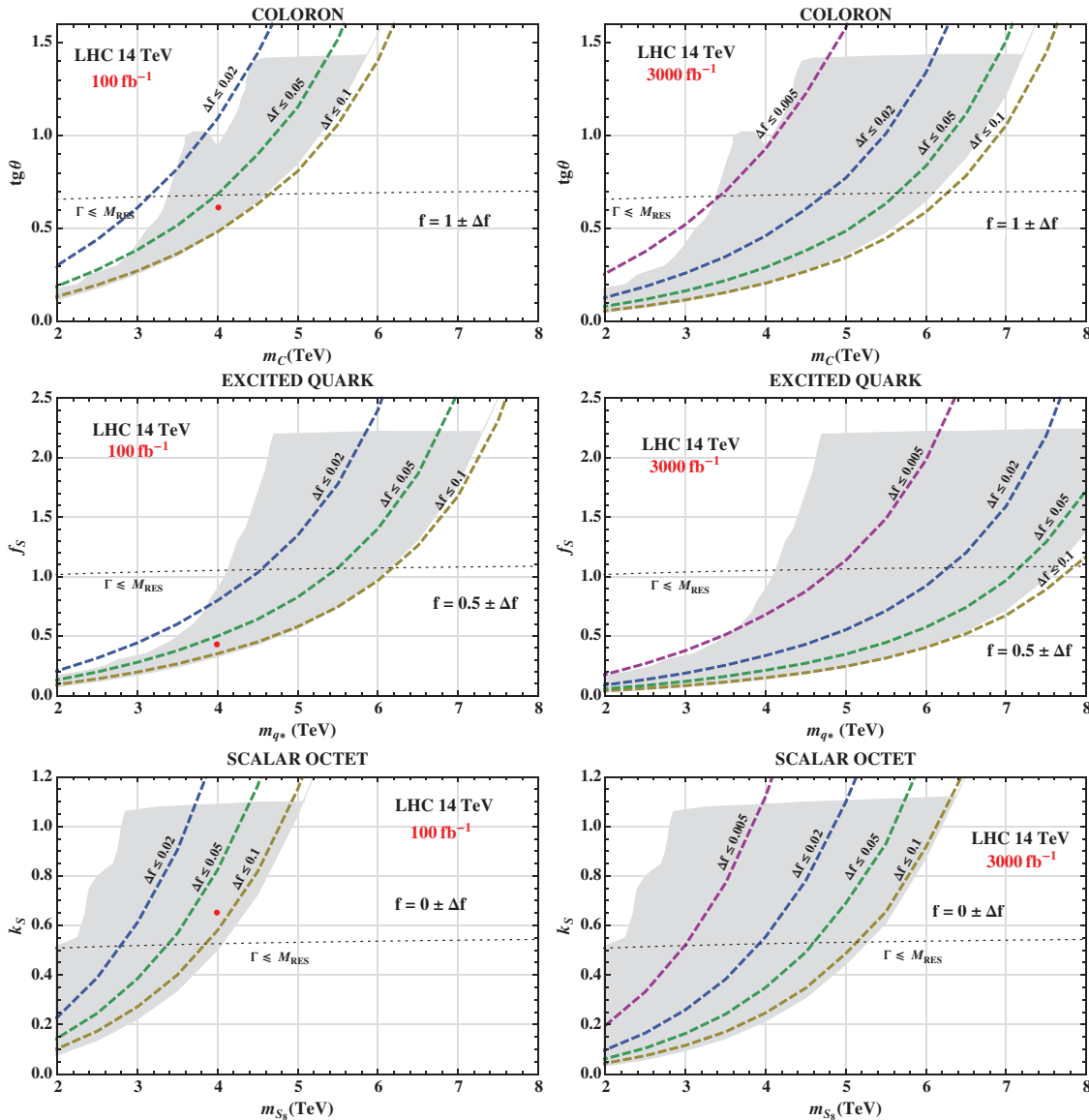

FIG. 5 (color). Contours of constant statistical uncertainty in the quark-jet signal fraction Δf (dashed lines) in the mass-coupling parameter space for the three dijet resonances at different 14 TeV LHC integrated luminosities (left plots: 100 fb^{-1}; right plots: 3000 fb^{-1}). The shaded regions show the areas that are allowed by the LHC-8 data, and where we can reach a 5σ discovery of the specific dijet resonance with the given luminosity. The dotted black line indicates the narrow-width limit; below this line, the color discriminant analysis is not possible but analysis of the JEPs is still valuable. In the case $L = 100$ fb^{-1} we also indicate with a red dot the mass-coupling values considered in the benchmark analyses of a $M = 4$ TeV dijet resonance, discussed in the text. Note that the use of JEPs can yield a statistically significant measurement distinguishing between the different types of resonances over the entire parameter space accessible to the LHC.

$$\Delta f \sim \frac{\sqrt{1 + 2\frac{B}{S}}}{\sqrt{S}} \qquad (23)$$

with the total number of signal (S) and background (B) events. $S = \sigma_S L$, $B = \sigma_B L$, where L is the integrated luminosity, σ_S is the dijet signal cross section (which depends on the resonance mass and coupling), and σ_B is the background cross section (which depends on the dijet invariant mass cut). As in the previous analysis at $M = 4$ TeV, we apply the CMS selection cuts in (10) and we restrict to a dijet invariant mass region $|M_{jj} - M| < \Gamma/2$, where, conservatively, we take $\Gamma = 0.15M$.

Through this analysis we can establish the region of masses and couplings where the quark jet-fraction parameter f can be measured sufficiently well to distinguish between colorons, excited quarks, and color-octet scalars. In particular, we obtain contours of constant statistical uncertainty in the signal quark-jet fraction, Δf, in the parameter space for the three dijet resonances at different 14 TeV LHC integrated luminosities, as shown in Fig. 5. Together with the Δf contours we show (in grey) the regions illustrated in Fig. 1, that are still allowed by LHC-8 data and where a 5σ discovery of the specific dijet resonance is achievable with the given luminosity. We also indicate the narrow-width limit where $\Gamma = M_{\mathrm{res}}$. Note that the region $\Gamma \leq M_{\mathrm{res}}$ which cannot be tested through the color discriminant variable can instead be explored by the analysis of JEPs. In the case $L = 100$ fb^{-1} we also indicate with a red dot the mass-coupling values considered in the analysis at $M = 4$ TeV. The corresponding f values and statistical sensitivities, we remind, are indicated in Tables I and II, respectively.

The results show that if a 5σ discovery of a dijet resonance occurs at the 14 TeV LHC, the statistical uncertainty on the corresponding f parameter will be small; we have $\Delta f \leq 0.1$ for all of the three types of resonances in essentially the entire relevant parameter space where we can reach a 5σ discovery at the 14 TeV LHC. Thus, it should be possible to use the analysis of JEPs to distinguish among gg, qg, and $\bar{q}q$ dijet resonances.

We must reiterate, however, that our study only examines the statistical significance of the dijet resonance discrimination through JEPs. We make no attempt to estimate the effects of possible systematic uncertainties on the JEPs, as this will require a detailed detector study and is only likely to be possible with data in hand—and is therefore beyond the scope of this paper.

VI. CONCLUSIONS

We have presented and analyzed two different strategies to reveal the nature of a dijet resonance at the 14 TeV LHC. The first method uses the recently introduced color discriminant variable, which can be constructed at the LHC from the measurements in the dijet channel of the signal cross section and of the resonance mass and width. The second strategy relies on the analysis of the energy profiles of the two final jets in the dijet channel. We have presented our results in the relevant mass vs coupling parameter space of $\bar{q}q$, qg, and gg resonances, where the resonances are still allowed by the 8 TeV LHC analyses and where a 5σ discovery in the dijet channel is achievable at the 14 TeV LHC (Fig. 1).

Figure 2 summarizes our results for discriminating among the three different types of resonances—a $\bar{q}q$ coloron, a qg excited quark, and a gg color-octet scalar—using the color discriminant variable, including estimated statistical and systematic uncertainties. We find that a qg excited quark can be cleanly distinguished from either a $\bar{q}q$ coloron or a gg color-octet scalar by the color discriminant variable at the 14 TeV LHC. Establishing the distinction between colorons and color-octet scalars using the color discriminant variable is more challenging, but we still find the possibility of a $\sim 2(3)\sigma$ separation for resonance masses of the order of 4(6) TeV.

A clearer distinction between $q\bar{q}$ and gg resonances can be achieved by applying our second strategy, the study of dijet energy profiles. Figure 5 summarizes our results for the analysis of the dijet energy profiles of $\bar{q}q$, qg, and gg resonances, including the statistical uncertainties and the effect of background subtraction. We find that the analysis of JEPs can distinguish gg, qg, and $\bar{q}q$ resonances even after accounting for statistical uncertainties in the signal and the background. The analysis of JEPs also has the advantage of being model independent, since it can provide information on the partonic composition of a dijet resonance regardless of the details of the model from which it arises.

We look forward to exciting results from the upcoming run of the LHC, and the possible discovery of a heavy dijet resonance.

[1] G. Aad *et al.* (ATLAS Collaboration), arXiv:1407.1376.
[2] CMS Collaboration, Report No. CMS-PAS-EXO-12-059.
[3] S. Chatrchyan *et al.* (CMS Collaboration), Phys. Rev. D **87,** 114015 (2013).
[4] Y. Gershtein *et al.*, arXiv:1311.0299.
[5] A. Atre, R. S. Chivukula, P. Ittisamai, and E. H. Simmons, Phys. Rev. D **88,** 055021 (2013).
[6] S. D. Ellis, Z. Kunszt, and D. E. Soper, Phys. Rev. Lett. **69,** 3615 (1992).
[7] E. H. Simmons, Phys. Rev. D **55,** 1678 (1997).
[8] R. S. Chivukula, A. G. Cohen, and E. H. Simmons, Phys. Lett. B **380,** 92 (1996).
[9] U. Baur, M. Spira, and P. M. Zerwas, Phys. Rev. D **42,** 815 (1990).
[10] U. Baur, I. Hinchliffe, and D. Zeppenfeld, Int. J. Mod. Phys. A **02,** 1285 (1987).
[11] T. Han, I. Lewis, and Z. Liu, J. High Energy Phys. 12 (2010) 085.
[12] H. n. Li, Z. Li, and C.-P. Yuan, Phys. Rev. Lett. **107,** 152001 (2011).
[13] H. n. Li, Z. Li, and C.-P. Yuan, Phys. Rev. D **87,** 074025 (2013).
[14] J. Gallicchio and M. D. Schwartz, Phys. Rev. Lett. **105,** 022001 (2010).
[15] J. Gallicchio and M. D. Schwartz, J. High Energy Phys. 10 (2011) 103.
[16] J. Gallicchio and M. D. Schwartz, Phys. Rev. Lett. **107,** 172001 (2011).
[17] S. Ozturk, Adv. High Energy Phys. **2014,** 1 (2014).
[18] A. J. Larkoski, J. Thaler, and W. J. Waalewijn, J. High Energy Phys. 11 (2014) 129.
[19] A. Altheimer *et al.*, J. Phys. G **39,** 063001 (2012).
[20] C. T. Hill, Phys. Lett. B **266,** 419 (1991).
[21] P. H. Frampton and S. L. Glashow, Phys. Lett. B **190,** 157 (1987).
[22] M. V. Martynov and A. D. Smirnov, Mod. Phys. Lett. A **24,** 1897 (2009).
[23] R. S. Chivukula, E. H. Simmons, and N. Vignaroli, Phys. Rev. D **87,** 075002 (2013).
[24] R. S. Chivukula, P. Ittisamai, and E. H. Simmons, arXiv:1406.2003.
[25] P. L. Cho and A. K. Leibovich, Phys. Rev. D **53,** 150 (1996).
[26] A. R. Zerwekh and R. Rosenfeld, Phys. Lett. B **503,** 325 (2001).
[27] R. S. Chivukula, A. Grant, and E. H. Simmons, Phys. Lett. B **521,** 239 (2001).
[28] R. S. Chivukula, A. Farzinnia, J. Ren, and E. H. Simmons, Phys. Rev. D **87,** 094011 (2013).

[29] M. Redi, V. Sanz, M. de Vries, and A. Weiler, J. High Energy Phys. 08 (2013) 008.
[30] R. S. Chivukula, E. H. Simmons, and N. Vignaroli, Phys. Rev. D **88,** 034006 (2013).
[31] Y. Bai and B. A. Dobrescu, J. High Energy Phys. 07 (2011) 100.
[32] R. M. Harris and K. Kousouris, Int. J. Mod. Phys. A **26,** 5005 (2011).
[33] V. Khachatryan *et al.* (CMS Collaboration), arXiv:1411.2646.
[34] N. Vignaroli, Phys. Rev. D **89,** 095027 (2014).
[35] C. Bini, R. Contino, and N. Vignaroli, J. High Energy Phys. 01 (2012) 157.
[36] D. Greco and D. Liu, J. High Energy Phys. 12 (2014) 126.
[37] M. Chala, J. Juknevich, G. Perez, and J. Santiago, J. High Energy Phys. 01 (2015) 092.
[38] F. Yu, arXiv:1308.1077.
[39] J. Alwall, M. Herquet, F. Maltoni, O. Mattelaer, and T. Stelzer, J. High Energy Phys. 06 (2011) 128.
[40] T. Sjostrand, S. Mrenna, and P. Z. Skands, Comput. Phys. Commun. **178,** 852 (2008).
[41] H. L. Lai, M. Guzzi, J. Huston, Z. Li, P. M. Nadolsky, J. Pumplin, and C.-P. Yuan, Phys. Rev. D **82,** 074024 (2010).
[42] N. D. Christensen and C. Duhr, Comput. Phys. Commun. **180,** 1614 (2009).
[43] B. A. Dobrescu and F. Yu, Phys. Rev. D **88,** 035021 (2013).
[44] A. D. Martin, W. J. Stirling, R. S. Thorne, and G. Watt, Eur. Phys. J. C **63,** (2009).
[45] J. Pumplin, D. R. Stump, J. Huston, H. L. Lai, P. M. Nadolsky, and W. K. Tung, J. High Energy Phys. 07 (2002) 012.
[46] K. Gumus, N. Akchurin, S. Esen, and R. M. Harris, Report No. CMS-NOTE-2006-070; Report No. CERN-CMS-NOTE-2006-070.
[47] V. Rentala, N. Vignaroli, H. n. Li, Z. Li, and C.-P. Yuan, Phys. Rev. D **88,** 073007 (2013).
[48] P. Agrawal and V. Rentala, J. High Energy Phys. 05 (2014) 098.
[49] ATLAS Collaboration, Report No. ATL-PHYS-PUB-2012-003; Report No. ATL-COM-PHYS-2012-738.
[50] G. Aad *et al.* (ATLAS Collaboration), Phys. Rev. D **83,** 052003 (2011).
[51] S. Chatrchyan *et al.* (CMS Collaboration), J. High Energy Phys. 06 (2012) 160.
[52] D. Acosta *et al.* (CDF Collaboration), Phys. Rev. D **71,** 112002 (2005).
[53] M. Cacciari, G. P. Salam, and G. Soyez, Eur. Phys. J. C **72,** 1896 (2012).